BBA - Molecular Basis of Disease 1865 (2019) 73–85

Contents lists available at ScienceDirect

BBA - Molecular Basis of Disease

journal homepage: www.elsevier.com/locate/bbadis

Methylglyoxal accumulation de-regulates HoxA5 expression, thereby impairing angiogenesis in glyoxalase 1 knock-down mouse aortic endothelial cells

Cecilia Nigro[a,b,1], Alessia Leone[a,b,1], Michele Longo[a,b], Immacolata Prevenzano[a,b], Thomas H. Fleming[c,d], Antonella Nicolò[a,b], Luca Parrillo[a,b], Rosa Spinelli[a,b], Pietro Formisano[a,b], Peter P. Nawroth[c,d], Francesco Beguinot[a,b], Claudia Miele[a,b,*]

[a] URT of the Institute of Experimental Endocrinology and Oncology "G. Salvatore", National Council of Research, Naples, Italy
[b] Department of Translational Medical Sciences, University of Naples "Federico II", Naples, Italy
[c] Department of Medicine I and Clinical Chemistry, Heidelberg University Hospital, Heidelberg, Germany
[d] German Center for Diabetes Research (DZD), Ingolstädter Landstraße 1, 85764 Neuherberg, Germany

ARTICLE INFO

Keywords:
Angiogenesis
Diabetes mellitus
Endothelial cells
Glyoxalase 1
HoxA5
Methylglyoxal

ABSTRACT

Impaired angiogenesis leads to long-term complications and is a major contributor of the high morbidity in patients with Diabetes Mellitus (DM). Methylglyoxal (MGO) is a glycolysis byproduct that accumulates in DM and is detoxified by the Glyoxalase 1 (Glo1). Several studies suggest that MGO contributes to vascular complications through mechanisms that remain to be elucidated. In this study we have clarified for the first time the molecular mechanism involved in the impairment of angiogenesis induced by MGO accumulation.

Angiogenesis was evaluated in mouse aortic endothelial cells isolated from Glo1-knockdown mice (Glo1KD MAECs) and their wild-type littermates (WT MAECs). Reduction in Glo1 expression led to an accumulation of MGO and MGO-modified proteins and impaired angiogenesis of Glo1KD MAECs. Both mRNA and protein levels of the anti-angiogenic HoxA5 gene were increased in Glo1KD MAECs and its silencing improved both their migration and invasion. Nuclear NF-κB-p65 was increased 2.5-fold in the Glo1KD as compared to WT MAECs. Interestingly, NF-κB-p65 binding to HoxA5 promoter was also 2-fold higher in Glo1KD MAECs and positively regulated HoxA5 expression in MAECs. Consistent with these data, both the exposure to a chemical inhibitor of Glo1 "SpBrBzGSHCp2" (GI) and to exogenous MGO led to the impairment of migration and the increase of HoxA5 mRNA and NF-κB-p65 protein levels in microvascular mouse coronary endothelial cells (MCECs).

This study demonstrates, for the first time, that MGO accumulation increases the antiangiogenic factor HoxA5 via NF-κB-p65, thereby impairing the angiogenic ability of endothelial cells.

1. Introduction

Angiogenesis is a vital process occurring in tissue development and wound healing in damaged tissues [1]. It is a multistep event that starts when endothelial cells (ECs) switch from "quiescent" to "angiogenic" phenotype in response to pro-angiogenic stimuli [2]. Following stimulation, ECs begin to proliferate, invade the extracellular matrix (ECM) thereby contributing to the formation of an immature capillary structure with deposition of a new basement membrane (BM) and pericytes recruitment [3]. Under physiological conditions, angiogenesis is a highly regulated process that is turned on for brief periods and then is completely inhibited [4]. The balanced activity between specific pro-

Abbreviations: AG, aminoguanidine; AGEs, advanced glycation end products; BM, basement membrane; DM, diabetes mellitus; DMSO, dimethyl sulfoxide; ECs, endothelial cells; ECM, extracellular matrix; FBS, fetal bovine serum; GAPDH, glyceraldehyde 3-phosphate dehydrogenase; GI, Glo1 inhibitor "SpBrBzGSHCp2"; Glo1, glyoxalase 1; Glo1KD, Glo1-knockdown; GTT, glucose tolerance test; HFD, high fat diet; HIF-1-alpha, hypoxia-inducible factor 1-alpha; ITT, insulin tolerance test; MAECs, mouse aortic endothelial cells; MCECs, mouse coronary artery endothelial cells; MGO, methylglyoxal; PARP, Poly (ADP-ribose) polymerase; qRT-PCR, real time quantitative reverse transcription PCR; RAGE, advanced glycation end products receptor; STD, standard diet; VEGF, vascular endothelial growth factor; VEGFR2, type 2 vascular endothelial growth factor receptor; WT, wild type

* Corresponding author at: URT of the Institute of Experimental Endocrinology and Oncology "G. Salvatore", National Council of Research, Naples, Italy.
E-mail address: c.miele@ieos.cnr.it (C. Miele).

[1] These authors equally contributed to this study.

https://doi.org/10.1016/j.bbadis.2018.10.014
Received 30 May 2018; Received in revised form 11 September 2018; Accepted 8 October 2018
Available online 18 October 2018
0925-4439/ © 2018 Elsevier B.V. All rights reserved.

and anti-angiogenic molecules which can activate or stop this process is critical for an optimal angiogenic response [3]. The persistent hyperglycemic milieu related to DM is associated with the onset and progression of micro- and macro-vascular complications, most of which are characterized by impaired vascularization and/or aberrant angiogenesis [5].

A wide number of studies performed both in animals and humans demonstrated that chronic hyperglycemia impairs endothelial function in macro- and micro-vasculature [6]. Indeed, through the activation of several molecular pathways, hyperglycemia induces excessive generation of ROS, increased oxidative stress and reduced vasodilation. Moreover, glucotoxicity induces a low-grade proinflammatory condition, due to the activation of transcription factors such as NF-κB [7].

In the last decade, great interest has been paid to MGO, a major precursor of advanced glycation end products (AGEs) in ECs [8]. MGO mainly originates as a byproduct of glycolysis by non-enzymatic degradation of triosephosphates [9], with a formation rate of about 125 μmol/kg cell mass per day under normoglycemic conditions [10]. The majority of MGO (> 99%) is detoxified by the glyoxalase system in healthy conditions [8]. The glyoxalase system is localized in the cytosol and includes two enzymes: the rate limiting enzyme Glo1 and the glyoxalase 2, beside a catalytic amount of reduced glutathione [11]. In diabetic patients, plasma MGO concentration is increased from 2- to 5-fold [12] as a consequence of a higher formation rate but also a reduced detoxification due to the down-regulation of both Glo1 expression and activity [13,14].

We have previously demonstrated that MGO induces endothelial dysfunction in vitro in aortic ECs and in vivo in C57BL/6 mice [15–17]. Other studies have also shown that high levels of MGO contribute to the development of cardiomyopathy by increasing inflammation and EC loss [18], by inducing vascular contractile dysfunction in arterial walls [19] as well as cell death via NF-κB activation in rat diabetic lens [20]. Moreover, emerging evidence has highlighted the harmful effect of MGO on angiogenesis. Indeed, it has been demonstrated that the exposure to MGO impairs viability, migration and tube formation of bovine aortic ECs [21], while the overexpression of Glo1 favours muscle reperfusion after ischemic insults in diabetic rats [22]. However, the molecular mechanisms underlying these effects remain to be elucidated.

Hox genes encode for a family of transcription factors highly conserved which act as master regulators of tissue and organ patterning [23]. Moreover, they play an essential role in regulating the function of vascular system. In particular, they coordinate the processes required for proper vascular formation during development, as well as the maintenance and repair of the vasculature system throughout life [24]. Hox gene family includes a number of genes with pro- or anti-angiogenic function. Among the anti-angiogenic Hox genes, it has been shown that HoxA5 blocks angiogenesis and increases vascular stability by the upregulation of anti-angiogenic factors, such as p53, and the downregulation of pro-angiogenic factors, including type 2 vascular endothelial growth factor receptor (VEGFR2) and Hif1alpha [25]. Arderiu G. et al. have shown that HoxA5 expression in ECs stabilizes adherens junctions through β-catenin retention [26], thus preventing the first step of angiogenesis.

In this study, we have investigated the role of Hox genes in the effect played by MGO accumulation on angiogenic process in ECs.

2. Materials and methods

2.1. Reagents

Media, sera and antibiotics for cell culture were from Lonza (Walkersville, MD, USA). Protein electrophoresis and Western blot reagents were from Bio-Rad (Richmond, VA, USA) and ECL reagents from Pierce (Rockford, USA). The used antibodies were anti-HoxA5, anti-14-3-3Θ, anti-MGO from Abcam (Cambridge, UK), anti-NF-κB-p65, anti-glyceraldehyde 3-phosphate dehydrogenase (GAPDH), anti-lamin A/C, anti-actin, anti-vinculin and anti-vascular endothelial growth factor (VEGF) from Santa Cruz Biotecnology (CA, USA), anti-α-tubulin and anti-poly (ADP-ribose) polymerase (PARP) from Sigma-Aldrich (St Luis, MO, USA), anti-caspase-3 and anti-VEGFR2 from Cell Signaling (Leiden, The Netherlands). TRIzol and SuperScript III were from Invitrogen (Carlsbad, CA, USA). SYBR Green Supermix was from Bio-Rad. NF-κB Activation Inhibitor (JSH-23) was from Santa Cruz Biotecnology. The miRNeasy Mini Kit and QIAquick PCR Purification kit were from QIAGEN (Hilden, Germany). All other chemicals were from Sigma-Aldrich.

2.2. Cell culture procedure

MAECs were isolated by Glo1KD mice and their WT littermates, as described in [27]. Glo1KD mice were kindly provided by M. Brownlee (Albert Einstein College of Medicine, Bronx, NY) and generated as described by El Osta A. et al. [28]. MAECs were cultured as previously described [15]. The absence of mycoplasma contamination was assessed by MycoAlert Detection Kit by Lonza. Where indicated, 4 mmol/L or 10 mmol/L Aminoguanidine (AG; Sigma-Aldrich) was added to the culture medium for 96 h. For the inhibition of NF-κB-p65, cells were treated with the inhibitor of NF-κB-p65 nuclear translocation JSH-23 60 μmol/L 16 h before cell harvesting.

SV40 immortalized MCECs were purchased from Biozol/CELLutions Biosystems Inc. (Catalogue No.CLU510). Cells were grown in DMEM media containing 1 g/L glucose supplemented with 10% FBS (fetal bovine serum), 1% penicillin-streptomycin and 1% HEPES and all growth surfaces were coated with 0.5% gelatin in PBS for 30 min at 37 °C prior to seeding. Where indicated, MCECs were treated either with MGO 500 μmol/L for 16 h or with GI 10 μmol/L for 48 h. Dimethyl sulfoxide (DMSO) was used as vehicle of GI.

2.3. Animals, diet and tolerance tests

Six-week-old C57BL/6 male mice were purchased from the Charles River Laboratories (Milan, Italy). The mice were housed in a temperature-controlled (22 °C) room with a 12 h light/dark cycle, in accordance with the Guide for the Care and Use of Laboratory Animals published by the National Institutes of Health (publication no. 85-23, revised 1996). Protocols were approved by the ethics committee of the "Federico II" University of Naples. Animals were fed with a high-fat diet (HFD) or a standard chow diet (STD) for 22 weeks and monitored as previously described [29]. For insulin tolerance test (ITT), mice were fasted for 4 h followed by insulin injection (0.75 U/kg body weight, i.p.). For glucose tolerance test (GTT), mice were fasted overnight and then injected with glucose (2 g/kg body weight, i.p.). Whole venous blood was obtained from the tail vein at 0, 15, 30, 45, 60, 90 and 120 min after the injection. Blood glucose was measured using an automatic glucometer (One Touch Lifescan, Milan, Italy). At the end of the study, mice were killed by cervical dislocation. Aortas were isolated, homogenized in QIAzol Lysis Reagent by the use of Tissue Lyser LT (QIAGEN) and RNA isolated as following described.

2.4. Mouse aortic ring assay

The assay was performed on aortic rings isolated from 8 weeks old WT and Glo1KD mice, as previously described [30]. Briefly, thoracic aortas were excised from mice and peri-vascular fibro-adipose tissue was removed under the stereomicroscope. Aortas were then cleaned and cut into 0.5-mm rings. They were serum starved overnight to equilibrate their growth factor responses. Then, two rings per well were transferred to a 24-well plate coated with 300 μL of Growth factor-reduced Matrigel (BD Biosciences, Franklin Lakes, NJ, USA) and overlaid with additional 300 μL of Matrigel.

The plates were incubated at 37 °C to allow Matrigel to polymerize

and 10% FBS was added to each well. Media were changed every 2 days. Aortic rings were examined daily, and digital images were taken on day 5 for analysis of vascular endothelial outgrowth (*sprouts*).

2.5. Cytoplasmic and nuclear fractionation

Nuclear and cytoplasmic proteins were extracted using the NE-PER Nuclear and Cytoplasmic Extraction Kit purchased from Thermo Fisher Scientific (Waltham, Massachusetts, USA), according to the manufacturer's instructions.

2.6. Western blot analysis

Total protein lysates were obtained and separated by SDS-PAGE as previously described [15]. Upon incubation with primary and secondary antibodies (for full list see above), immmunoreactive bands were detected by chemiluminescence and densitometric analysis was performed using ImageJ software.

2.7. RNA isolation and real time quantitative reverse transcription PCR (qRT-PCR)

Total RNA was isolated from cells and tissues using TRIzol Reagent and miRNeasy Mini Kit (QIAGEN), respectively, according to the manufacturer's protocol. After quantification with NanoDrop 2000 spectrophotometer (Thermo Fisher Scientific), 1 μg of total RNA was reverse transcribed using SuperScript III according to the manufacturer's instructions. The differential expression of genes were analyzed by real time-PCR, as previously described [31], and quantified as relative expression units using the comparative $2^{-\Delta\Delta Ct}$ method for the analysis of gene expression in cells and the $2^{-\Delta Ct}$ method for the analysis of gene expression in mice [32]. Cyclophilin A was used as housekeeping gene. Specific primers used for amplification were purchased from Sigma-Aldrich and listed below:

Cyclophilin A:	Forward 5'-GCAGACAAAGTTCCAAAGACAG- 3'
	Reverse 5'-CACCCTGGCACATGAATCC- 3'
Glo1:	Forward 5'-CCCTCGTGGATTTGGTCACA-3'
	Reverse 5'-AGCCGTCAGGGTCTTGAATG-3'
HoxA5:	Forward 5'-CCCAGATCTACCCCTGGATG-3'
	Reverse 5'-CAGGGTCTGGTAGCGAGTGT-3'
HoxD10:	Forward 5'-GGCCTTCCAGAAGACAGGA-3'
	Reverse 5'- GTGAGCCAATTGCTGGTTGG-3'
HoxA3:	Forward 5'- CCGCGGTCTGAAGGCTAC-3'
	Reverse 5'- -TGAACCAGGAATGGTCTCC-3'
HoxA9:	Forward 5' -AAACCTGAACCGCTCTCGG-3'
	Reverse 5' -GTGTAGGGGCATCGCTTCTT-3'
HoxB3:	Forward 5' -AAGTGTTAGCCGTCTCTCCG-3'
	Reverse 5' -TATTCACATCGAGCCCCAGC-3'
Chip-HoxA5:	Forward 5'-ACACACAGGTTTTCTCCCCA-3'
	Reverse 5'-GAATTTGATGGCGAGGGACC-3'
NF-κB-p65:	Forward 5'-CTGATGTGCATCGGCAAGTG -3'
	Reverse 5'-CTCTTCAATCCGGTGGCGAT-3'

2.8. Cell transfection

1×10^5 MAECs were seeded in 60-mm plates. After 24 h, cells were transfected with 5 nmol/L HoxA5 siRNA (Origene, Rockville, MD, USA) or negative control (scramble) and incubated with complete medium for 48 h. TransIT-X2 (Mirus Bio LCC, Madison, WI, USA) was used as transfection reagent, according to the manufacturer's instructions.

2.9. Measurement of MGO

Intracellular MGO concentration was measured in WT and Glo1KD MAECs extracts by HPLC after derivatization with 1,2-diamino-4,5-dimethoxybenzene as previously described [33].

2.10. Cell growth assay

5×10^4 cells were seeded in MW-6 and cell growth was monitored at 0 (18 h from plating), 12, 24, 48, 72, 96 h by automated cell count with TC10TM Automated Cell Counter (Bio-Rad).

2.11. Transwell migration and invasion assays

Cells were serum starved for 5 h. After trypsinization, 1×10^5 cells/well were plated on the upper side of 12-well cell culture inserts (BD Biosciences) with 5 μm pores polycarbonate membrane for the evaluation of migration in MAECs and with polyethylene terephthalate (PET) in MCECs. To perform invasion assay, 12-well cell culture inserts with 8 μm pores PET membrane were coated with 100 μL of Matrigel (BD Biosciences). Culture medium with or without 10% FBS was added to the bottom of the well, as chemotactic stimulus. Following an overnight incubation for MAECs or 48 h of incubation for MCECs, the top of the insert was cleared of cells with a cotton swab; the top and the bottom of insert were washed 3 times with 1× PBS. Inserts were incubated 30 min at room temperature with 11% glutaraldehyde to fix the cells migrated to the lower side of the insert, and then washed 3 times with 1× PBS. Cells were then stained with Crystal Violet and washed with 1× PBS. Cells from 4 representative fields from each insert were counted.

2.12. Chromatin immunoprecipitation assay

5×10^5 cells were fixed for 10 min at room temperature with 1% (v/v) formaldehyde and crosslinking reaction was stopped with 125 mmol/L glycine for 5 min. Formaldehyde and glycine were removed by centrifugation (3 min at 13,000 rpm). SDS and HBSS buffer were added to the cells and the DNA was sonicated using the Bioruptor® sonicator (Diagenode, Seraing, Belgium). Cellular debris was removed by centrifugation, then equal amount of DNA was immunoprecipitated using anti-NF-κB-p65 antibody (Santa Cruz Biotecnology) and with anti-mouse IgG beads (Thermo Fisher Scientific). Immuneprecipitated fragments were washed with dialysis buffer, IP wash buffer and TE buffer. Fragments were eluted at 37 °C for 45 min with elution buffer and then de-crosslinked O.N. with 5 mol/L NaCl at 65 °C. Proteins were removed using proteinase K and 1 mol/L Tris-HCl/0.5 mol/L EDTA. The immunoprecipitated DNA was purified with QIAquick PCR Purification Kit according to the manufacturer's instructions, and quantified by Real-Time PCR using specific primer sets flanking the expected p65 binding site on HoxA5 promoter.

2.13. Cloning strategy and luciferase assay

NF-κB-p65 binding site on HoxA5 promoter was amplified by PCR using the following primers: forward primer: 5′-Kpn1GAATTGGCCCT GCTGCTG-3′ and reverse primer: 5′-Sac1GAATTTGATGGCGAGGG ACC-3′, where Kpn1 and Sac1 indicate the restriction sites added to the sequence. The purified fragment was cloned into the pGL3 luciferase promoter vector (Promega, Madison WI, USA). Amplification of the reporter construct was performed using DH5 alpha *E. coli* cells (New England Biolabs). 250 ng reporter construct (pGL3 NF-κB-p65 binding site) was transfected in Hela cells in presence or not of 250 ng NF-κB-

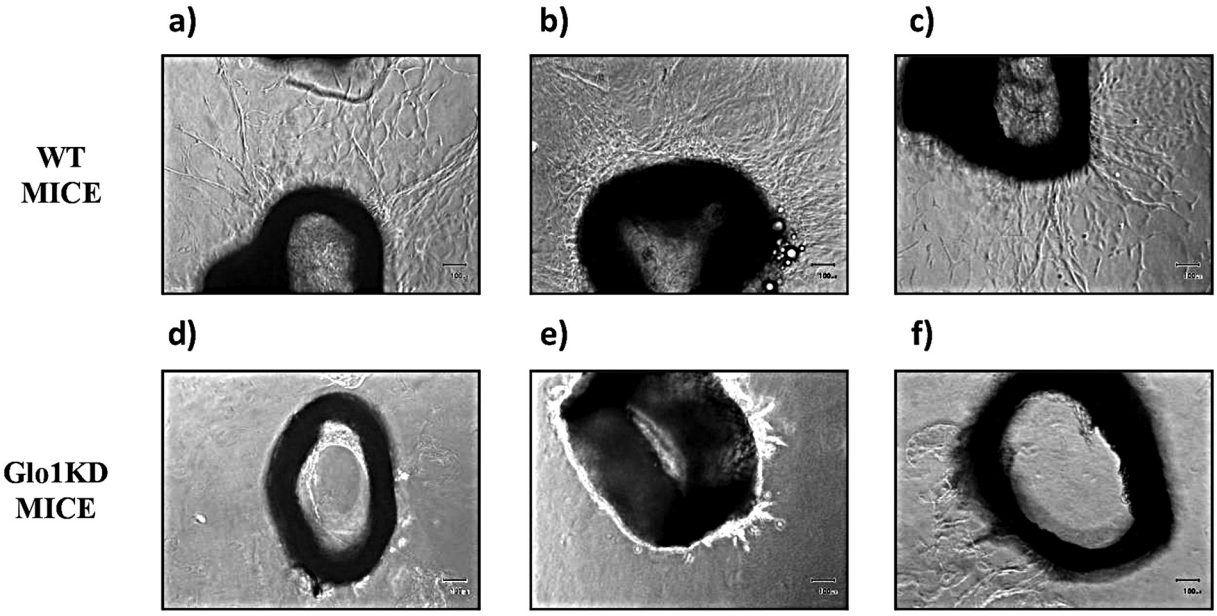

Fig. 1. Formation of tube-like structures of EC sprouting from aortic rings of WT and Glo1KD mice. Tube formation by ECs was monitored ex vivo in aortic rings isolated from mice (n = 5) and embedded in Matrigel. Representative images of aortic rings from three 8-week old WT (**a–c**) and three age-matched Glo1KD (**d–f**) mice on day 5 after embedding are reported at 10× magnification.

p65-pRc/CMV vector. To normalize the luciferase activity, 50 ng of a control plasmid encoding a Renilla luciferase gene was cotransfected into the cells. After 24 h, cell lysates were assayed for Firefly and Renilla luciferase activity using a single luciferase reporter assay kit, according to the manufacturer's instructions.

2.14. Statistical procedures

Data are expressed as means ± SD or ± SEM as indicated. All experiments were performed at least three times. Comparison between groups was performed using Student's *t*-test. A p value of < 0.05 was considered statistically significant.

3. Results

3.1. Effect of Glo1KD on angiogenesis in MAECs

Angiogenesis has been assessed ex vivo in the aortic rings from Glo1KD mice and their WT littermates by sprouting assay. As shown by the images in Fig. 1, tube formation of ECs sprouting from the aortic rings of Glo1KD mice (panels d–f) is impaired compared to the aortic rings of WT mice (panels a–c).

MAECs isolated from the aortae of Glo1KD and WT mice have been characterized by measuring both Glo1 expression and MGO concentration. As shown in Fig. 2a, Glo1 mRNA levels are reduced by 50% in Glo1KD MAECs compared to WT MAECs. This reduction is paralleled by a 5-fold increase of intracellular MGO concentration (Fig. 2b) and a 1.5-fold increase of MGO-modified proteins (Fig. 2c and d), in Glo1KD MAECs as compared to WT MAECs. Treatment of Glo1KD MAECs with 10 mmol/L AG for 96 h is able to reduce the formation of MGO-modified proteins (Fig. 2c and d).

The main steps of the angiogenic process, i.e. proliferation, migration and invasion, have been then separately investigated in vitro (Fig. 3). Glo1KD MAECs are characterized by a slower cell growth compared to WT MAECs. The proliferation, indicated as fold of cell number over time 0, is significantly reduced in Glo1KD MAECs starting from 48 h (Fig. 3a). The cleavage of Caspase-3 and its downstream target PARP have been evaluated as apoptosis marker (Fig. S1), indicating that the reduced proliferation of Glo1KD MAECs is not dependent on apoptosis.

Migration ability of MAECs has been quantified as the fold increase of migrated cell number in response to 10% FBS, used as pro-angiogenic stimulus, over the number of migrated cells in the absence of FBS (*basal*). Migration of WT MAECs is ca. 8-fold increased in response to FBS. Conversely, this ability is increased by only 2-fold in response to FBS in Glo1KD MAECs (Fig. 3b). Moreover, while FBS induces a ca. 6-fold increase of invasion in WT MAECs, Glo1KD MAECs are not able to invade the Matrigel-coated membrane following exposure to FBS (Fig. 3c). Thus, both migration and invasion are significantly impaired in Glo1KD MAECs compared to WT MAECs.

3.2. HoxA5 involvement in Glo1KD mediated impairment of angiogenesis in MAECs

The expression levels of anti- and pro- angiogenic Hox genes, known to be expressed in adulthood, have been measured in WT and Glo1KD MAECs and are reported in Table 1.

Among these, mRNA levels of HoxA5, which plays an anti-angiogenic function, are ca. 2-fold higher in Glo1KD as compared to WT MAECs (Table 1). Similarly, also protein levels of HoxA5 are 2-fold increased in Glo1KD MAECs (Fig. 4) and are associated with a 40% reduction of VEGFR2 protein, which is known to be a down-regulated target of HoxA5 (Fig. S2a, b). Conversely, the protein levels of its ligand, VEGF, do not change in WT and Glo1KD MAECs (Fig. S2c, d).

Interestingly, chronic treatment with AG significantly reduces HoxA5 protein levels in Glo1KD MAECs (Fig. 4).

To prove the involvement of HoxA5 in Glo1KD dependent impairment of angiogenesis, HoxA5 expression has been transiently silenced by the use of specific siRNAs. HoxA5 expression levels in scramble-transfected Glo1KD MAECs are increased by ca. 1.6-fold as compared to scramble-transfected WT MAECs (Fig. 5a). The transfection of 5 nmol/L HoxA5 siRNA induces a 50% reduction of HoxA5 expression in Glo1KD MAECs (Fig. 5a), thus lowering HoxA5 expression in Glo1KD MAECs to a similar extent of control scramble-transfected WT MAECs. Interestingly, HoxA5 silencing is able to improve both migration (Fig. 5b) and invasion (Fig. 5c) ability of Glo1KD MAECs.

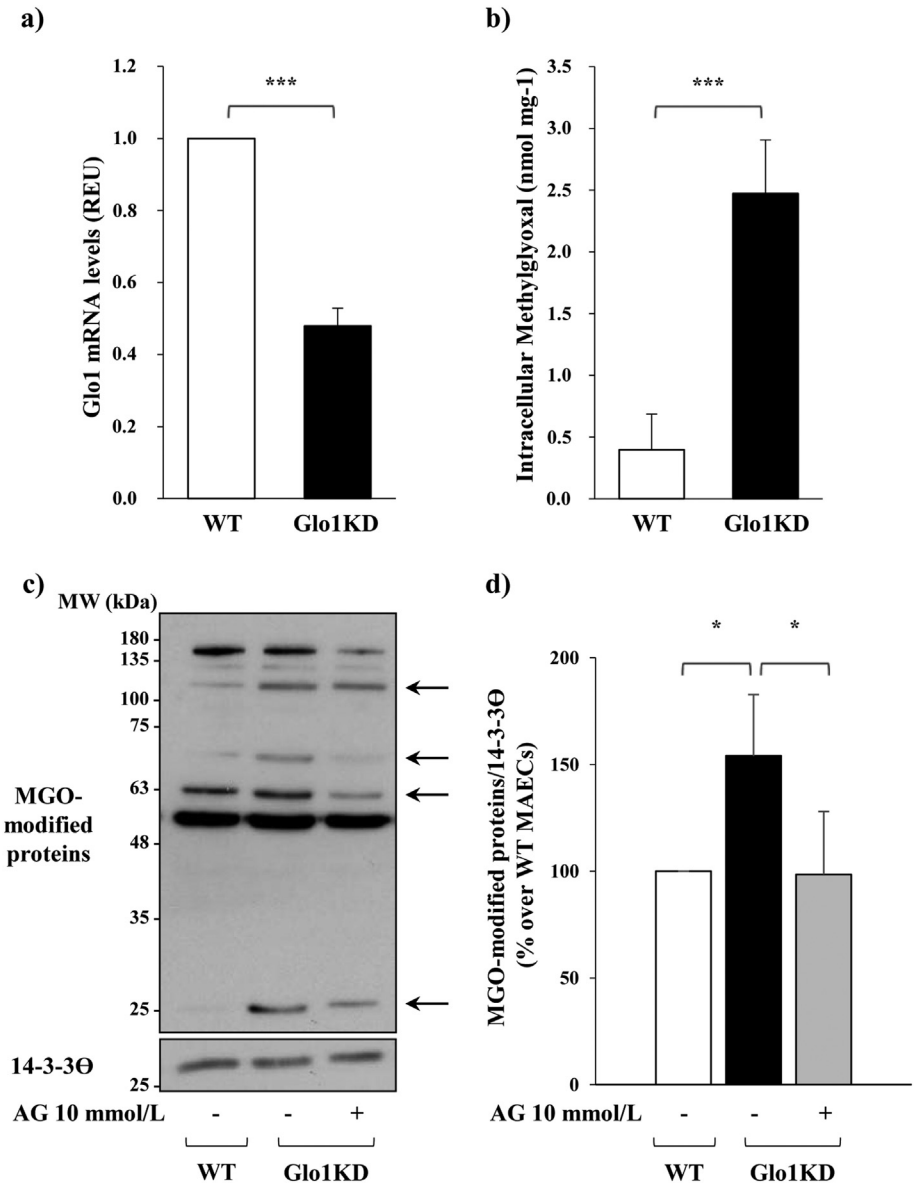

Fig. 2. Glo1 expression, MGO and MGO-modified protein levels in WT and Glo1KD MAECs. **a**) Glo1 expression was analyzed by qRT-PCR (n = 6). The bars in the graph represent the mean ± SD of the expression units relative to Cyclophilin A, used as housekeeping gene. **b**) MGO intracellular concentration was measured by HPLC (n = 3). **c**) Intracellular formation of MGO-modified proteins was evaluated by Western blot on protein lysates of WT and Glo1KD MAECs treated or not with the MGO scavenger AG (10 mmol/L for 96 h), using anti-MGO antibody. Bands in (**c**), indicated by the arrows on the right side of the blot, show a spectrum of proteins of different molecular weight that are modified by MGO. Anti-14-3-3Θ antibody was used as loading control. **d**) MGO-modified protein levels were quantified by the densitometric analysis of each sample lane, normalized on the 14-3-3Θ specific band. The bars in the graph represent the mean ± SD (n = 3). Statistical analysis was evaluated using the Student's *t*-test; * $p \leq 0.05$, *** $p \leq 0.001$.

3.3. NF-κB-p65 role in the regulation of MGO induced HoxA5 overexpression

As possible regulator of HoxA5 expression, the levels of the transcription factor NF-κB-p65 have been evaluated in total protein lysates of Glo1KD and WT MAECs. The Glo1KD MAECs show an increase of ca. 2-fold in NF-κB-p65, which is reverted by chronic treatment with AG (Fig. 6a). Fractionation of nuclear from total protein lysates reveals a 1.5-fold increase of NF-κB-p65 in the cytosolic compartment (Fig. 6b) and a 2.5-fold increase of NF-κB-p65 in the nucleus of Glo1KD MAECs as compared to WT MAECs (Fig. 6c).

Next, to test the binding of NF-κB-p65 to HoxA5 promoter, a chromatin immunoprecipitation assay has been performed. A bioinformatic analysis (*http://jaspar.genereg.net/*) highlighted several predicted NF-κB-p65 binding sites on HoxA5 promoter. Chromatin from WT and Glo1KD MAECs has been immunoprecipitated with a NF-κB-p65 specific antibody and the putative highest scored binding sequence has been amplified by qRT-PCR to verify and quantify the binding of NF-κB-p65 to the HoxA5 promoter.

NF-κB-p65 binds HoxA5 promoter in WT MAECs and this binding is 2-fold higher in Glo1KD MAECs (Fig. 7a). Furthermore, luciferase activity is increased when NF-kB-p65 is co-transfected with the vector (pGL3 promoter) where NF-kB-p65 binding site (bs) is cloned (Fig. 7b). Interestingly, the inhibition of NF-κB-p65 obtained by the use of a NF-κB-p65 nuclear translocation inhibitor, JSH-23, is able to reduce HoxA5 mRNA expression in both WT and Glo1KD MAECs (Fig. 7c).

3.4. Effect of MGO in microvascular ECs

MCECs were used as microvascular EC line and both the exposure to exogenous MGO and the treatment with GI were performed to test the effect of MGO increase, as previously reported [15,34]. Migration ability of MCECs is significantly increased in response to FBS. Conversely, migration is impaired in MCECs treated either with MGO (Fig. 8a) or GI (Fig. 8b). Moreover, NF-κB-p65 protein levels are increased in MCECs treated with MGO, compared to not treated control cells (Fig. 8c), as well as in MCECs treated with GI, compared to both not treated and vehicle-treated control cells (Fig. 8d). NF-κB-p65 increase associates with a 1.4-fold increase of HoxA5 expression in MCECs treated either with MGO (Fig. 8e) or with GI (Fig. 8f).

These data indicate that migration is impaired by MGO also in microvascular ECs and this associates with the up-regulation of NF-κB-p65

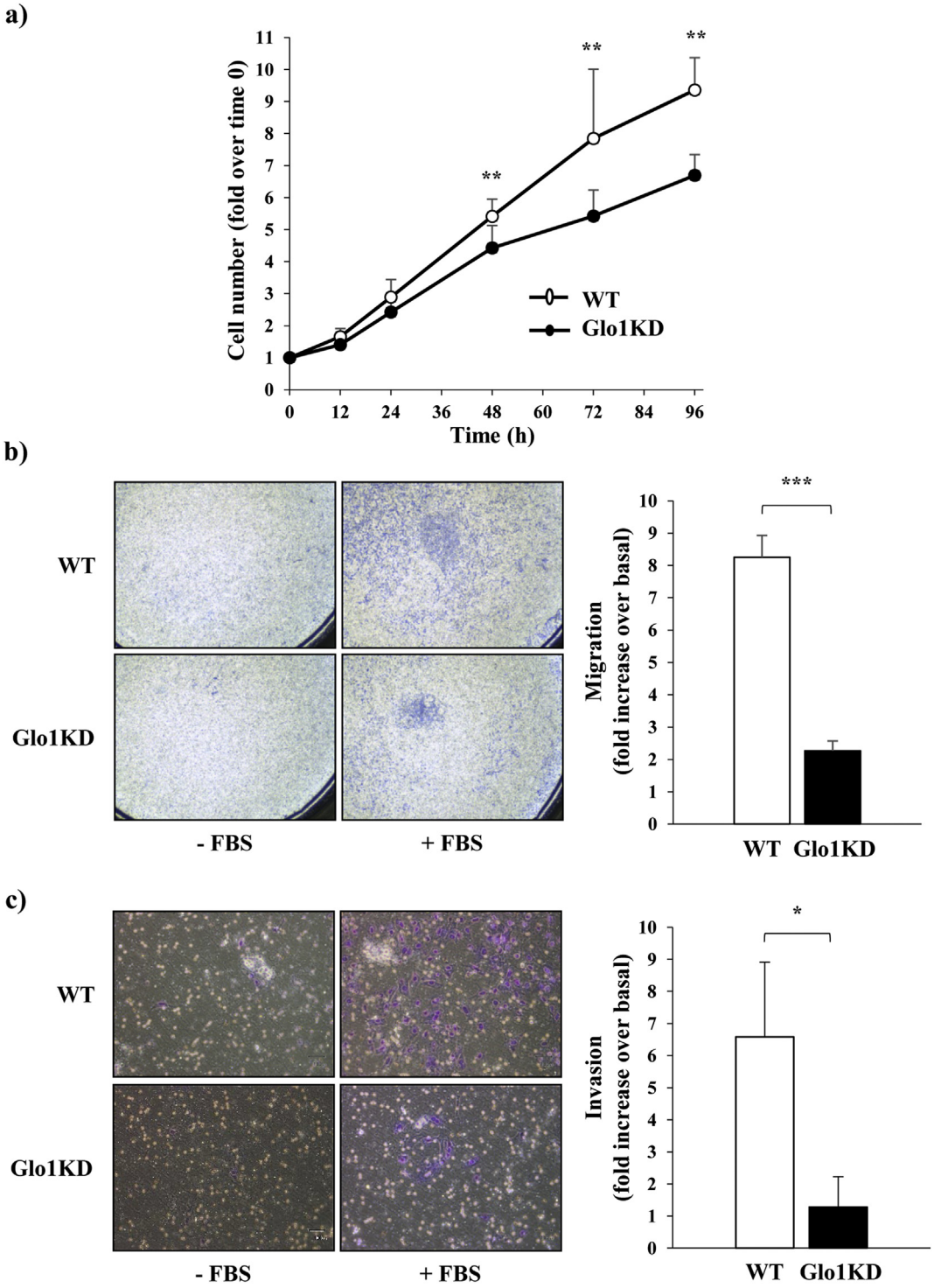

Fig. 3. Cell growth, migration and invasion assays in WT and Glo1KD MAECs. **a**) Cell growth of WT (n = 3) and Glo1KD MAECs (n = 3) was tested from time 0 to 96 h by automated cell counter and reported in the graph as fold of cell number over time 0. **b**) Cells were seeded on the upper side of a 5 μm transwell insert and migration ability was tested in presence or not of 10% FBS. Migrated cells were stained with crystal violet and are visible as violet dots in the 4× magnification images on the left. **c**) Invasion was tested evaluating the ability of cells to pass through a 8 μm transwell insert coated with Matrigel, in presence or not of 10% FBS. Representative 10× magnification images are on the left. The graphs on the right of panels (**b**) and (**c**) represent the mean ± SEM of the fold increase of migrated cells (n = 3) (**b**) or cells that passed through the matrigel and then the transwell insert (n = 5) (**c**), in response to 10% FBS over the basal migration (**b**) or invasion (**c**) in absence of 10% FBS. Statistical analysis was evaluated using the Student's *t*-test; $*p \leq 0.05$, $**p \leq 0.01$, $***p \leq 0.001$.

and HoxA5, as already demonstrated in macrovascular MAECs.

3.5. Expression levels of HoxA5 and NF-κB-p65 in vivo in a model of DM

Vascular tissue from HFD-fed mice was used to validate in an in vivo model of DM the expression of the molecular players shown to be crucial in the MGO-induced alteration of angiogenesis. As reported in Table 2, HFD-fed mice show higher body weight and glycaemia, develop glucose intolerance and insulin resistance as demonstrated by glucose and insulin tolerance tests, respectively. More interestingly, the

Table 1
mRNA levels of Hox genes. The expression of pro- and anti-angiogenic Hox genes was evaluated in MAECs by qRT-PCR. mRNA levels in Glo1KD MAECs are shown as the mean ± SD of the expression units relative to WT MAECs (REU). Cyclophilin A was used as housekeeping gene. Data were obtained from 8 (HoxD10, HoxA3, HoxA9, HoxB3) and 12 (HoxA5) independent experiments. Statistical analysis was evaluated using the Student's *t*-test.

	mRNA expression (REU)	*p* value
Anti-angiogenic genes		
HoxA5	1.87 ± 0.37	0.00000003
HoxD10	1.16 ± 0.77	n.s.
Pro-angiogenic genes		
HoxA3	2.21 ± 1.48	n.s.
HoxA9	1.54 ± 1.1	n.s.
HoxB3	1.03 ± 0.56	n.s.

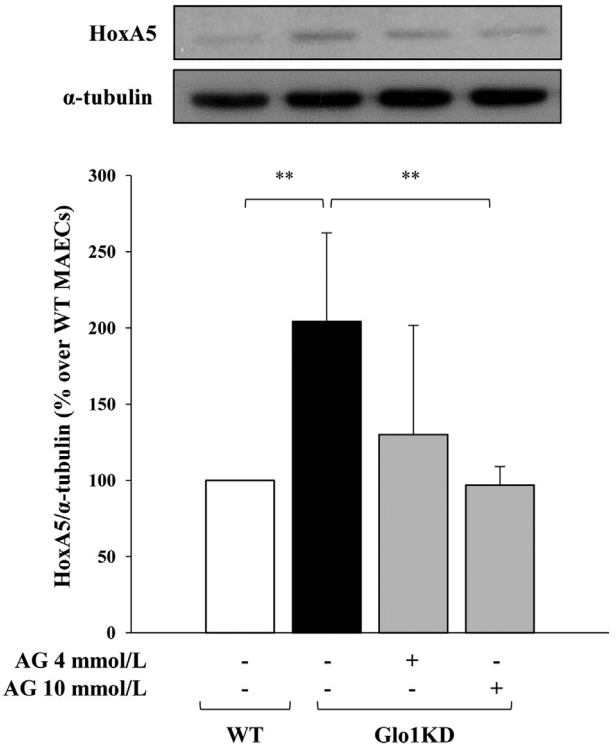

Fig. 4. Protein levels of the antiangiogenic factor HoxA5 in WT and Glo1KD MAECs. Protein lysates obtained by WT and Glo1KD MAECs, treated with 4 or 10 mmol/L AG for 96 h, were analyzed by Western blot with anti-HoxA5 antibody (n = 4). Anti-α-tubulin antibody was used as loading control. Protein levels were quantified by the densitometric analysis of four independent experiments. The bars in the graph represent the mean ± SD. Statistical analysis was evaluated using the Student's *t*-test; ** $p \leq 0.01$.

expression of both HoxA5 and NF-κB-p65 is significantly increased in the aortic vascular tissue from HFD-fed mice compared to STD control mice (Table 2).

4. Discussion

Diabetic vascular complications are associated with angiogenesis abnormalities. Given the complexity of these alterations, although extensive research has been performed, the mechanisms underlying the dysfunctional angiogenesis occurring in diabetes are still not fully understood [5]. In the present work, we identify HoxA5 as a new player in the impairment of angiogenesis observed in Glo1KD MAECs.

Previous studies performed in rats have shown that MGO exposure leads to the impairment of wound healing and the development of diabetes-like vascular damage. In particular, MGO treatment is associated with cell growth arrest, impaired vasodilation and degenerative changes in cutaneous microvessels with loss of ECs [35]. Moreover, it has been demonstrated that the overexpression of Glo1 inhibits AGEs formation in bovine ECs [36] and is able to improve hyperglycemia-induced impairment of angiogenesis in human microvascular ECs [37]. Here, for the first time, we have used a pathophysiological system in which an endogenous accumulation of MGO occurs into the cell as consequence of insufficient detoxification by Glo1, to investigate the effect of MGO overload on angiogenesis ex vivo.

MGO levels have been described to be increased from 2 to 5-fold in diabetic patients [12]. The reduced expression of Glo1 in Glo1KD MAECs associates with a 5-fold increase of endogenous MGO concentration, thus resulting in an increase of MGO accumulation similar to that found in diabetic subjects. Therefore, the use of this model, as well as the inhibition of Glo1 activity by GI in MCECs, allows us to bypass the supraphysiological effect linked to the treatment with high levels of exogenous MGO. Notably, a physiological reduction of Glo1 occurs with age and delays wound healing in old mice [38].

Although recent evidence proposes a previously unrecognized role of other detoxifying enzymes, such as aldose reductase, in the compensation for Glo1 loss [39], we show that the partial deletion of Glo1 is detrimental for the angiogenic function of ECs ex vivo. Indeed, in our experimental model, aortae isolated from Glo1KD mice feature an impaired EC sprouting ex vivo. The availability of MAECs isolated from this novel model gave us the possibility to investigate in detail the mechanistic aspects of Glo1KD effects on angiogenesis, also confirmed in microvascular MCECs following their treatment with GI or the exposure to MGO. Angiogenesis is a complex highly regulated process, involving EC proliferation, matrix degradation, cell migration, tube formation and vessel maturation [1,40]. Isolated Glo1KD MAECs show a reduced cell growth compared to WT MAECs. Although others have provided evidence of a pro-apoptotic effect of MGO [41–43], in our system the reduced cell growth is not dependent on cell apoptosis, as demonstrated by the lack of Caspase-3 and PARP cleavage in Glo1KD MAECs. This suggests that the delay in cell growth depends on a decrease in cell proliferation. Glo1KD MAECs also show an impaired ability to invade an ECM extract and migrate through a porous membrane in response to a pro-angiogenic stimulus, indicating that the partial depletion of Glo1 is responsible for the impairment of different steps of the angiogenic process in MAECs.

Given the essential role played by genes belonging to the Hox gene family in regulating physiological processes in adult tissues, including angiogenesis and wound healing [44], we have focused on them as candidate mediators of the observed phenotype in Glo1KD MAECs. Among the Hox genes analyzed, we have found an overexpression of the anti-angiogenic HoxA5 in Glo1KD as compared to WT MAECs. The ability of AG to rescue HoxA5 levels would suggest that its overexpression is a consequence of a MGO-mediated effect. Recent evidence have demonstrated that murine hemangioma cell growth is reduced by sustained HoxA5 expression [26], which is also associated to retinoic acid-induced cell growth inhibition, acting as a downstream mediator of retinoic acid receptor-β [45]. Moreover, HoxA5 has growth-suppressive properties through the activation of p53 expression [46]. Although these studies highlight a negative effect of HoxA5 on cell growth, we hypothesize that it may play a role also in the invasion process. Indeed, migration and invasion tests performed in this study have been carried out in a time span of 18 h, which is lower than that necessary to observe the significant delay of cell growth (48 h) in Glo1KD MAECs. Moreover, VEGFR2 protein levels are reduced in Glo1KD MAECs, as expected. Indeed, VEGFR2 has been reported to be a down-regulated target of HoxA5 [25] and the reduction of its protein levels have also been associated to the inhibition of Glo1 [21].

The obtained data suggest that HoxA5 may represent a good target for answering the question of which mediator may be involved in the angiogenesis impairment observed in our model. Indeed, both

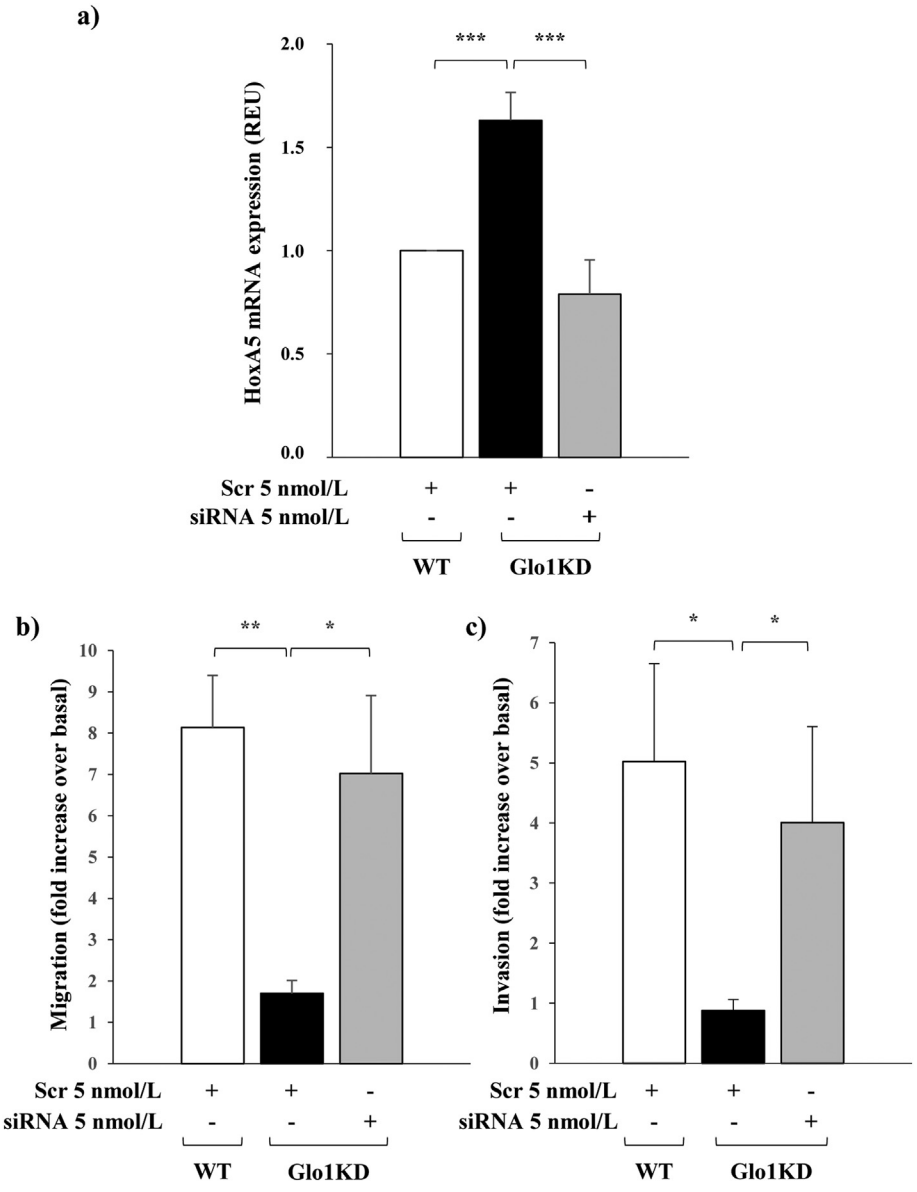

Fig. 5. Effect of HoxA5 silencing on migration and invasion ability of Glo1KD MAECs. MAECs were transfected with 5 nmol/L of negative control (scr) or HoxA5 siRNA (siRNA) where indicated. **a**) HoxA5 mRNA levels were measured by qRT-PCR (n = 3). The bars in the graph represent the mean ± SD of the expression units relative to Cyclophilin A, used as housekeeping gene. Migration (**b**) and invasion (**c**) were evaluated as reported in Fig. 3 legend in scramble and HoxA5 siRNA transfected cells (n = 3). Bars in the graphs show the fold increase of migration and invasion in presence of 10% FBS over the basal condition (w/o FBS). Statistical analysis was evaluated using the Student's *t*-test; $*p \leq 0.05$, $** p \leq 0.01$, $*** p \leq 0.001$.

migration and invasion ability of Glo1KD MAECs are improved by HoxA5 silencing. This is the first study proving the involvement of HoxA5 on impaired angiogenesis as a consequence of MGO accumulation in MAECs. Moreover, the molecular events occurring between MGO accumulation and HoxA5 overexpression has also been investigated.

Hox gene expression is commonly regulated via several mechanisms including microRNAs action, methylation and transcription factor-mediated regulation [44]. In our cell model, the expression of *HoxA5* was not dependent upon either promoter de-methylation nor by microRNAs known to have *HoxA5* as target (data not shown). Nevertheless, we identified several predicted binding sites for the pro-inflammatory transcription factor NF-κB-p65, by a bioinformatic prediction search.

Activation of NF-κB-p65 is well known to contribute to the development of chronic disorders, such as diabetes and its associated complications. Indeed, hyperglycemia-mediated vascular complications involve the activation of several biochemical cascades that have been largely investigated in the last decades, including pro-inflammatory pathways [47]. Bierhaus et al. have demonstrated that ligands of the receptor for AGEs (RAGE) induce sustained activation of NF-κB-p65 both in vitro and in vivo, promoting the production of factors involved in the accelerated vascular disease [48]. Furthermore, it has been recently demonstrated a direct activation of NF-κB-p65 translocation by MGO in synovial cells [49].

Accordingly to the increase of NF-kB-p65 expression reported by El Osta et al. [28] in Glo1KD MAECs, our data demonstrate that NF-κB-p65 protein levels are higher in Glo1KD than in WT MAECs. This increase is lost when Glo1KD MAECs are chronically exposed to the MGO scavenger AG, which directly reacts with MGO, thus preventing the MGO-derived AGEs formation and its damaging downstream effects. Moreover, NF-kB-p65 is more activated in Glo1KD compared to WT MAECs. These data are strengthened by previous studies in rats and diabetic patients, demonstrating that the activation of NF-kB-p65 is associated with an increase of its expression, and the new synthesis of NF-kB-p65 itself is critical for maintaining the chronic NF-kB-p65 activation [48].

Even though our work is based on a peculiar model which allows the investigation of the specific MGO effect on endothelial cell function, we also used a HFD-fed mouse model recapitulating the diabetic condition (i.e. hyperglycaemia, impaired glucose tolerance and insulin resistance) to confirm the up-regulation of both NF-κB-p65 and HoxA5

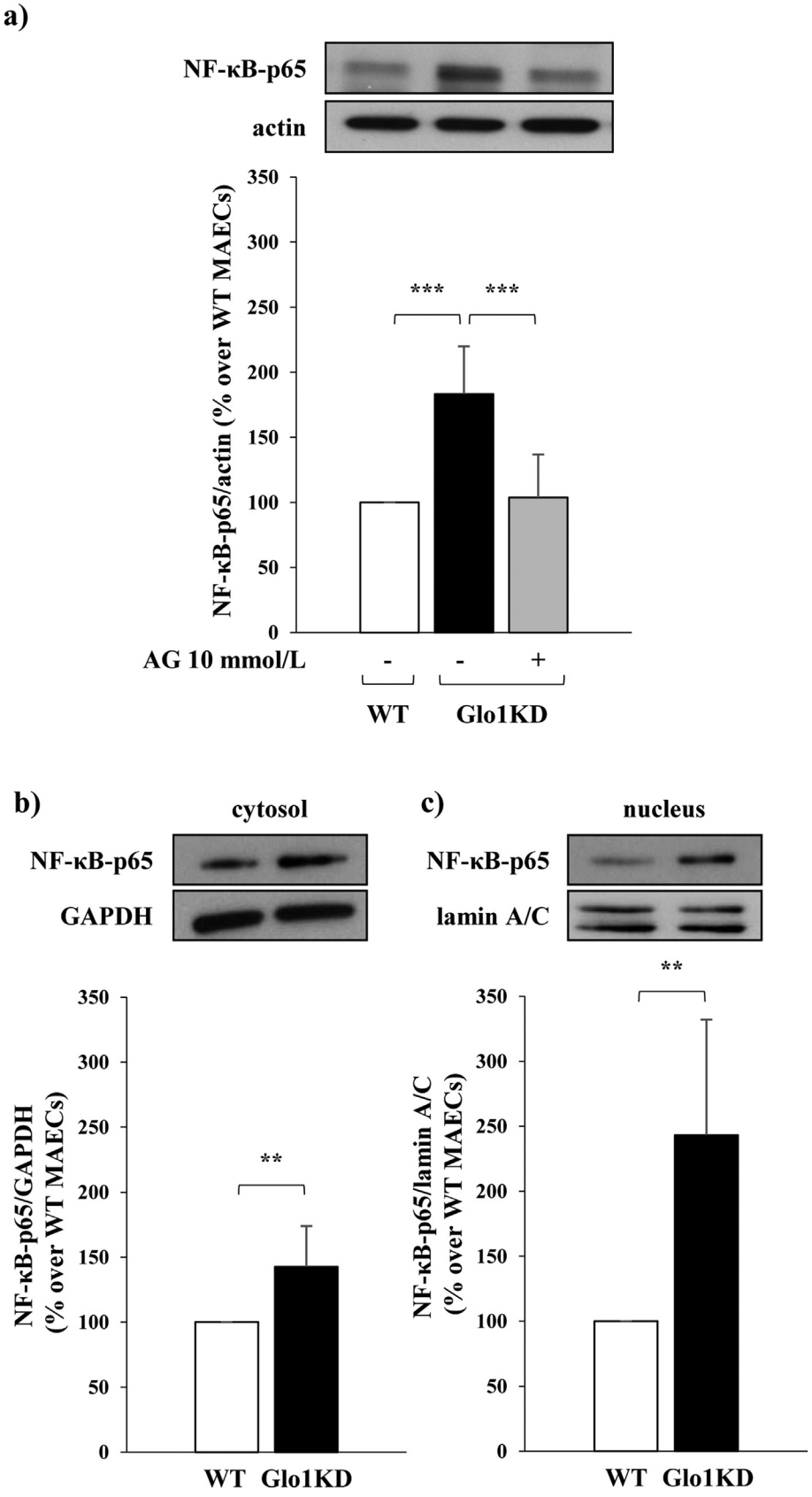

Fig. 6. NF-κB-p65 levels in WT and Glo1KD MAECs. **a**) Whole cell protein lysates from WT and Glo1KD MAECs were analyzed by Western blot with anti-NF-κB-p65 and anti-actin antibodies (n = 9). (**b**, **c**) Protein lysates from cytoplasmic/nuclear fractionation were evaluated by Western blot with anti-NF-κB-p65 antibody (n = 6). Cytoplasmic protein normalization was performed using anti-GAPDH antibody (**b**), nuclear protein normalization with anti-lamin A/C antibody (**c**). The bars in the graphs represent the mean ± SD. Statistical analysis was evaluated using the Student's *t*-test; $^{**}p \leq 0.01$, $^{***}p \leq 0.001$.

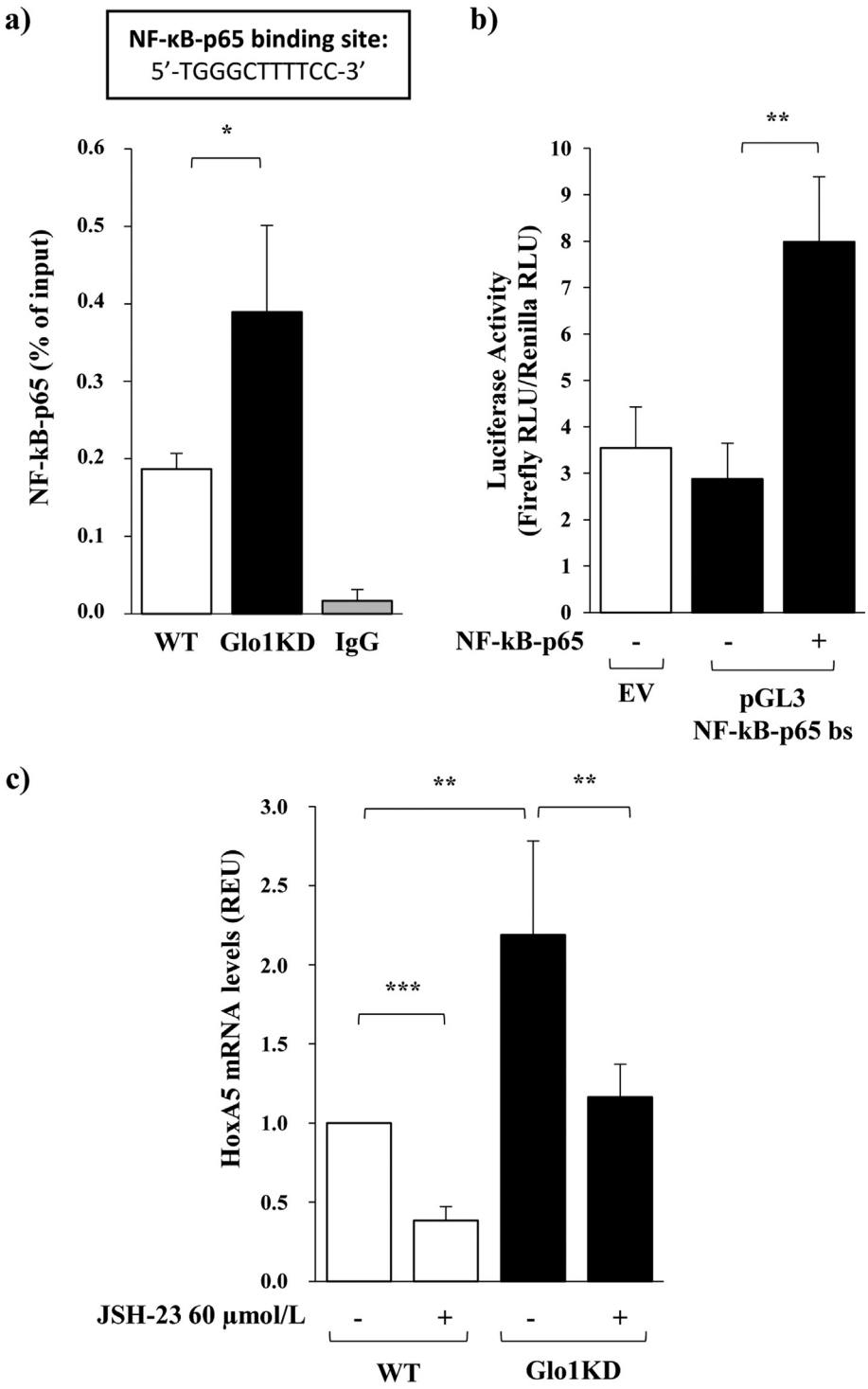

Fig. 7. NF-κB-p65-dependent regulation of HoxA5 transcription. **a**) NF-κB-p65 binding on HoxA5 promoter was tested by chromatin immunoprecipitation assay (ChIP) followed by quantization by qRT-PCR of a putative high scored NF-κB-p65-consensus sequence on HoxA5 promoter (5′-TGGGCTTTTCC-3′) reported at the top of the panel. Bars in the graph represent a quantitation of the HoxA5 promoter region bound by NF-κB-p65 and are shown as the percent (%) of chromatin recovered by ChIP ± SEM of five independent experiments. **b**) The luciferase activity of empty pGL3 promoter (EV) and pGL3 promoter containing NF-κB-p65 binding site (pGL3 NF-κB-p65 bs), co-transfected or not with 250 ng NF-κB-p65 pRc/CMV vector, was measured by luciferase assay. Luciferase activity was measured in relative light units (RLU). Bars in the graph represent the mean ± SD of Firefly luciferase activity normalized on Renilla luciferase activity, obtained from three independent experiments. **c**) Cells were treated with the NF-κB-p65 inhibitor JSH-23 (60 µmol/L) and HoxA5 mRNA levels were analyzed by qRT-PCR (n = 5). Cyclophilin A was used as housekeeping gene. Statistical analysis was evaluated using the Student's *t*-test; $^{*}p \leq 0.05$, $^{**}p \leq 0.01$, $^{***}p \leq 0.001$.

in vivo in the vascular tissue. It has been previously reported that HFD increases the tissue accumulation of MGO and MGO-derived AGEs in rodents [50–52]. Moreover, HFD is known to impair angiogenesis, both in hind limb reperfusion and wound healing models in mice [53–55], thus indicating the HFD-fed mouse as a suitable model to confirm the molecular alterations observed in vitro in ECs. Although a systemic up-regulation of NF-kB-p65 may be expected in HFD, this is the first evidence of HoxA5 over-expression in the vascular tissue of HFD-fed mice.

Within the anti-angiogenic context, NF-kB-p65 activation may be seen as paradoxical. However, it is noteworthy that while in tumor cells NF-kB-p65 is mostly oncogenic, its upregulation in ECs is associated with angiostatic activity [56]. Indeed, besides exerting a negative effect on ECM degradation [57] and tube formation [58], NF-kB activation in ECs induces the expression of not only angiogenic (e.g. VEGF) but also angiostatic factors (e.g. VEGI) [56]. As a potential mechanism in the activation of NF-kB, we hypothesize that MGO-induced oxidative stress may be causative of NF-kB-p65 activation [59], as suggested by our preliminary data proving a protective effect of the anti-oxidative agent *N*-acetyl cysteine (data not shown). Conversely, the hypothesis that MGO-dependent AGE/RAGE pathway [48] or Glo1KD related NF-kB-p65 epigenetic modification (i.e. H3K4me1) [28] could also be the cause for increased NF-kB-p65 in our model requires further

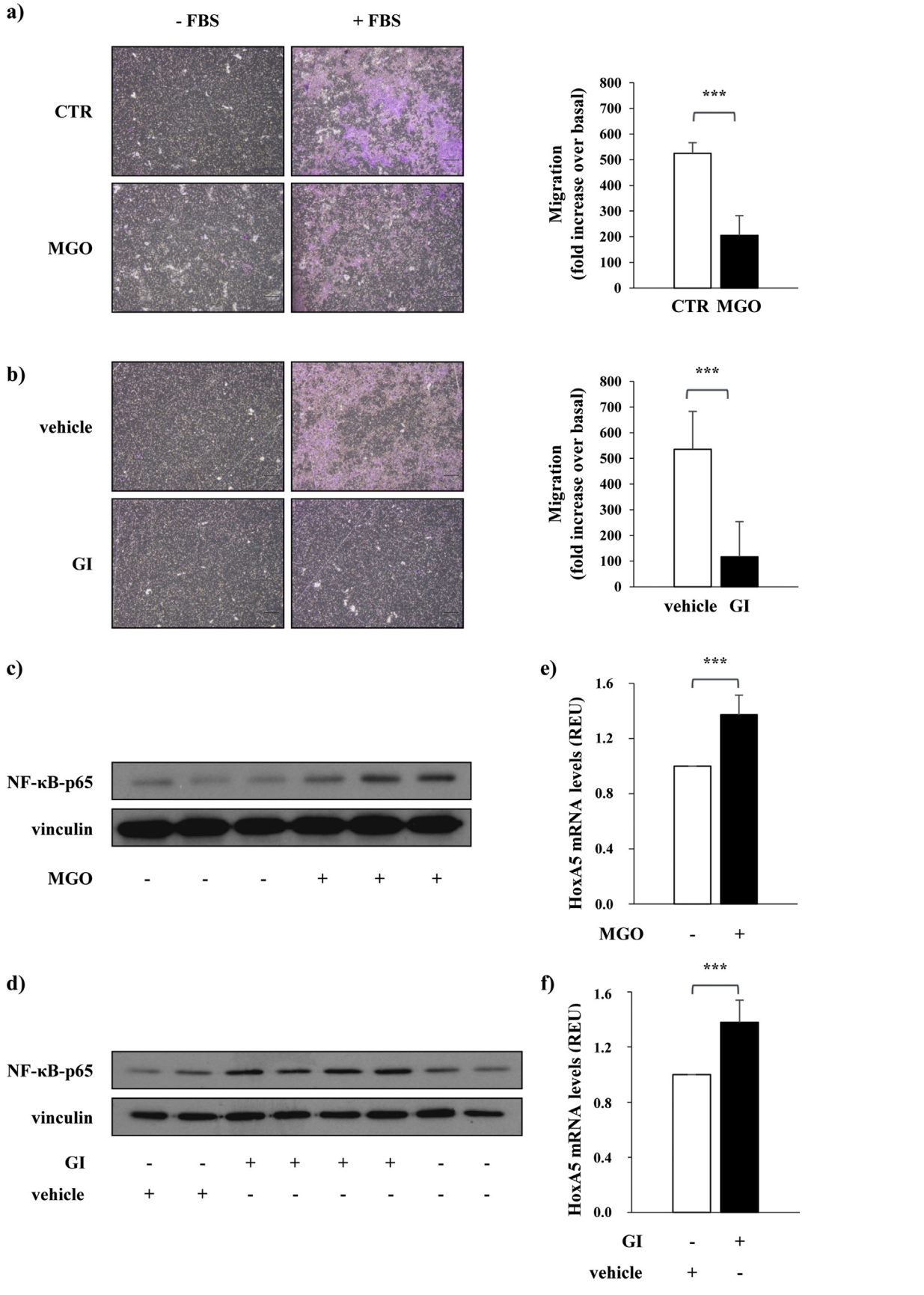

(caption on next page)

Fig. 8. Effect of MGO in MCECs. MCECs were exposed to MGO (500 μmol/L) for 16 h (**a**, **c** and **e**) or to GI (10 μmol/L) for 48 h (**b**, **d** and **f**). The vehicle of the GI was DMSO and used to treat control cells. Each experiment was performed in triplicate. **a**, **b**) After treatment, MCECs were seeded on the upper side of a 5 μm transwell insert and migration ability was tested in presence or not of 10% FBS. Migrated cells were stained with crystal violet and are visible as violet dots in the 4× magnification images on the left. The graphs on the right of panels (**a**) and (**b**) represent the mean ± SD of the fold increase of migrated cells in response to 10% FBS over the basal migration in absence of FBS. **c**, **d**) Whole cell protein lysates were analyzed by Western blot with anti-NF-κB-p65 and anti-vinculin antibodies. **e**, **f**) HoxA5 mRNA levels were measured by qRT-PCR. The bars in the graphs represent the mean ± SD of the expression units relative to Cyclophilin A, used as housekeeping gene. Statistical analysis was evaluated using the Student's *t*-test; $^{***}p \leq 0.001$.

Table 2
Expression levels of HoxA5 and NF-κB-p65 in HFD-fed mice. C57BL/6 mice were fed with HFD (n = 7) or STD (n = 7) for 22 weeks. At the end of diet protocol, body weight and fasting glycaemia were analyzed. Glucose tolerance and insulin resistance were determined by GTT and ITT, respectively, and are shown in the table as the area under the curve (AUC). mRNA levels of HoxA5 and NF-κB-p65 were measured in the vascular tissue by qRT-PCR and are reported as $2^{-\Delta Ct}$ (arbitrary units, AU). *p* value was calculated by Student's *t*-test.

	STD	HFD	*p* value
Body weight (g)	34.5 ± 2.5	44.6 ± 4.3	0.0001
Glycaemia (mg/dL)	105.7 ± 8.7	162.4 ± 31.0	0.0005
GTT AUC (mg/dL × min)	7,967 ± 1053	18,423 ± 6225	0.0009
ITT AUC (mg/dL × min)	9,954 ± 1473	13,888 ± 1761	0.0007
HoxA5 (AU)	0.018 ± 0.002	0.024 ± 0.003	0.01
NF-κB-p65 (AU)	0.075 ± 0.005	0.113 ± 0.021	0.0007

investigation.

Our study provides the first evidence that NF-κB-p65 binds *HoxA5* promoter in MAECs. HoxA5 binding by NF-κB-p65 is higher in Glo1KD MAECs as compared to WT MAECs. Moreover, NF-κB-p65 binding to the promoter positively regulates the expression of the anti-angiogenic *HoxA5* in MAECs. Although this study is mostly based on MAECs, which are considered macrovascular ECs, we also demonstrate here that MGO impairs the migration ability and induces the up-regulation of both HoxA5 and NF-κB-p65 in MCECs, indicating that similar damaging effects of MGO on the angiogenic function, found in MAECs, also occurs in microvascular ECs.

5. Conclusion

This study provides a novel mechanism in the understanding of the damaging specific effect of Glo1 reduction and concurrent MGO accumulation on angiogenesis, in a normoglycemic microenvironment. Through the activation of the transcription factor NF-κB-p65, MGO accumulation induces the overexpression of HoxA5 leading to the impairment of angiogenesis.

The results obtained in this study emphasize the need of identifying novel strategies able to interfere with these molecular events for the prevention and treatment of diabetes associated microvascular complications.

Supplementary data to this article can be found online at https://doi.org/10.1016/j.bbadis.2018.10.014.

Transparency document

The Transparency document associated with this article can be found, in online version.

Acknowledgements

This study was funded by the European Foundation for the Study of Diabetes (EFSD)/Novo Nordisk (2015–2017) and by the Ministero dell'Istruzione, dell'Università e della Ricerca Scientifica (grants PRIN, PON 01_02460 and POR 03PE_00060_8 Campania Bioscience). This study was supported in part by the FLAGSHIP "InterOmics" Project ASPIRE, funded and supported by the Italian MIUR and CNR organizations. ML and LP are the recipients of the SID/FO.DI.RI.-MSD ITALIA 2017 Research Fellowship. TF was supported by the Deutsche Forschungsgemeinschaft (DFG; SFB1118). We are grateful to M. Brownlee (Albert Einstein College of Medicine, Bronx, NY, USA) for having enable us to use the Glo1-KD mice. We thank Antonio D'Andrea for his technical support.

References

[1] P. Carmeliet, Angiogenesis in life, disease and medicine, Nature 438 (7070) (2005) 932–936.
[2] D. Ribatti, B. Nico, E. Crivellato, Morphological and molecular aspects of physiological vascular morphogenesis, Angiogenesis 12 (2) (2009) 101–111.
[3] A. Neve, et al., Extracellular matrix modulates angiogenesis in physiological and pathological conditions, Biomed. Res. Int. 2014 (2014) 756078.
[4] J. Folkman, Y. Shing, Angiogenesis, J. Biol. Chem. 267 (16) (1992) 10931–10934.
[5] J. Ribot, et al., Type 2 diabetes alters mesenchymal stem cell secretome composition and angiogenic properties, J. Cell. Mol. Med. 21 (2) (2017) 349–363.
[6] C.M. Sena, A.M. Pereira, R. Seica, Endothelial dysfunction - a major mediator of diabetic vascular disease, Biochim. Biophys. Acta 1832 (12) (2013) 2216–2231.
[7] M. Brownlee, The pathobiology of diabetic complications: a unifying mechanism, Diabetes 54 (6) (2005) 1615–1625.
[8] D.E. Maessen, C.D. Stehouwer, C.G. Schalkwijk, The role of methylglyoxal and the glyoxalase system in diabetes and other age-related diseases, Clin. Sci. (Lond.) 128 (12) (2015) 839–861.
[9] S.A. Phillips, P.J. Thornalley, The formation of methylglyoxal from triose phosphates. Investigation using a specific assay for methylglyoxal, Eur. J. Biochem. 212 (1) (1993) 101–105.
[10] P.J. Thornalley, Modification of the glyoxalase system in human red blood cells by glucose in vitro, Biochem. J. 254 (3) (1988) 751–755.
[11] P.J. Thornalley, The glyoxalase system in health and disease, Mol. Asp. Med. 14 (4) (1993) 287–371.
[12] A.C. McLellan, et al., Glyoxalase system in clinical diabetes mellitus and correlation with diabetic complications, Clin. Sci. (Lond.) 87 (1) (1994) 21–29.
[13] N. Rabbani, P.J. Thornalley, The critical role of methylglyoxal and glyoxalase 1 in diabetic nephropathy, Diabetes 63 (1) (2014) 50–52.
[14] A. Bierhaus, et al., Methylglyoxal modification of Nav1.8 facilitates nociceptive neuron firing and causes hyperalgesia in diabetic neuropathy, Nat. Med. 18 (6) (2012) 926–933.
[15] C. Nigro, et al., Methylglyoxal impairs endothelial insulin sensitivity both in vitro and in vivo, Diabetologia 57 (7) (2014) 1485–1494.
[16] P. Mirra, et al., The role of miR-190a in methylglyoxal-induced insulin resistance in endothelial cells, Biochim. Biophys. Acta 1863 (2) (2017) 440–449.
[17] C. Nigro, et al., miR-214-Dependent increase of PHLPP2 levels mediates the impairment of insulin-stimulated Akt activation in mouse aortic endothelial cells exposed to methylglyoxal, Int. J. Mol. Sci. 19 (2) (2018).
[18] B. Vulesevic, et al., Methylglyoxal-induced endothelial cell loss and inflammation contribute to the development of diabetic cardiomyopathy, Diabetes 65 (6) (2016) 1699–1713.
[19] M. Mukohda, et al., Methylglyoxal accumulation in arterial walls causes vascular contractile dysfunction in spontaneously hypertensive rats, J. Pharmacol. Sci. 120 (1) (2012) 26–35.
[20] J. Kim, et al., Accumulation of argpyrimidine, a methylglyoxal-derived advanced glycation end product, increases apoptosis of lens epithelial cells both in vitro and in vivo, Exp. Mol. Med. 44 (2) (2012) 167–175.
[21] H. Liu, et al., Angiogenesis impairment in diabetes: role of methylglyoxal-induced receptor for advanced glycation endproducts, autophagy and vascular endothelial growth factor receptor 2, PLoS One 7 (10) (2012) e46720.
[22] O. Brouwers, et al., Glyoxalase-1 overexpression partially prevents diabetes-induced impaired arteriogenesis in a rat hindlimb ligation model, Glycoconj. J. 33 (4) (2016) 627–630.
[23] R. Krumlauf, Hox genes in vertebrate development, Cell 78 (2) (1994) 191–201.
[24] J.M. Douville, J.T. Wigle, Regulation and function of homeodomain proteins in the embryonic and adult vascular systems, Can. J. Physiol. Pharmacol. 85 (1) (2007) 55–65.
[25] K. Rhoads, et al., A role for Hox A5 in regulating angiogenesis and vascular patterning, Lymphat. Res. Biol. 3 (4) (2005) 240–252.
[26] G. Arderiu, et al., HoxA5 stabilizes adherens junctions via increased Akt1, Cell Adhes. Migr. 1 (4) (2007) 185–195.
[27] F.M. Marelli-Berg, et al., Isolation of endothelial cells from murine tissue, J. Immunol. Methods 244 (1–2) (2000) 205–215.
[28] A. El-Osta, et al., Transient high glucose causes persistent epigenetic changes and altered gene expression during subsequent normoglycemia, J. Exp. Med. 205 (10) (2008) 2409–2417.

[29] G.A. Raciti, et al., Specific CpG hyper-methylation leads to Ankrd26 gene down-regulation in white adipose tissue of a mouse model of diet-induced obesity, Sci. Rep. 7 (2017) 43526.
[30] M. Baker, et al., Use of the mouse aortic ring assay to study angiogenesis, Nat. Protoc. 7 (1) (2011) 89–104.
[31] F. Oriente, et al., PREP1 deficiency downregulates hepatic lipogenesis and attenuates steatohepatitis in mice, Diabetologia 56 (12) (2013) 2713–2722.
[32] T.D. Schmittgen, K.J. Livak, Analyzing real-time PCR data by the comparative C-T method, Nat. Protoc. 3 (6) (2008) 1101–1108.
[33] A.C. McLellan, S.A. Phillips, P.J. Thornalley, The assay of methylglyoxal in biological systems by derivatization with 1,2-diamino-4,5-dimethoxybenzene, Anal. Biochem. 206 (1) (1992) 17–23.
[34] P.J. Thornalley, et al., Antitumour activity of S-p-bromobenzylglutathione cyclopentyl diester in vitro and in vivo. Inhibition of glyoxalase I and induction of apoptosis, Biochem. Pharmacol. 51 (10) (1996) 1365–1372.
[35] J. Berlanga, et al., Methylglyoxal administration induces diabetes-like microvascular changes and perturbs the healing process of cutaneous wounds, Clin. Sci. (Lond.) 109 (1) (2005) 83–95.
[36] M. Shinohara, et al., Overexpression of glyoxalase-I in bovine endothelial cells inhibits intracellular advanced glycation endproduct formation and prevents hyperglycemia-induced increases in macromolecular endocytosis, J. Clin. Invest. 101 (5) (1998) 1142–1147.
[37] U. Ahmed, et al., Reversal of hyperglycemia-induced angiogenesis deficit of human endothelial cells by overexpression of glyoxalase 1 in vitro, Ann. N. Y. Acad. Sci. 1126 (2008) 262–264.
[38] T.H. Fleming, et al., Aging-dependent reduction in glyoxalase 1 delays wound healing, Gerontology 59 (5) (2013) 427–437.
[39] J. Morgenstern, et al., Loss of glyoxalase 1 induces compensatory mechanism to achieve dicarbonyl detoxification in mammalian Schwann cells, J. Biol. Chem. 292 (8) (2017) 3224–3238.
[40] L. Lamalice, F. Le Boeuf, J. Huot, Endothelial cell migration during angiogenesis, Circ. Res. 100 (6) (2007) 782–794.
[41] M. Do, et al., delta-Tocopherol prevents methylglyoxal-induced apoptosis by reducing ROS generation and inhibiting apoptotic signaling cascades in human umbilical vein endothelial cells, Food Funct. 6 (5) (2015) 1568–1577.
[42] M. Fukunaga, et al., Methylglyoxal induces apoptosis through activation of p38 MAPK in rat Schwann cells, Biochem. Biophys. Res. Commun. 320 (3) (2004) 689–695.
[43] K. Seo, S.H. Ki, S.M. Shin, Methylglyoxal induces mitochondrial dysfunction and cell death in liver, Toxicol. Res. 30 (3) (2014) 193–198.
[44] S. Kachgal, K.A. Mace, N.J. Boudreau, The dual roles of homeobox genes in vascularization and wound healing, Cell Adhes. Migr. 6 (6) (2012) 457–470.
[45] H. Chen, et al., HOXA5 acts directly downstream of retinoic acid receptor beta and contributes to retinoic acid-induced apoptosis and growth inhibition, Cancer Res. 67 (17) (2007) 8007–8013.
[46] V. Raman, et al., Compromised HOXA5 function can limit p53 expression in human breast tumours, Nature 405 (6789) (2000) 974–978.
[47] J.L. Evans, et al., Oxidative stress and stress-activated signaling pathways: a unifying hypothesis of type 2 diabetes, Endocr. Rev. 23 (5) (2002) 599–622.
[48] A. Bierhaus, et al., Diabetes-associated sustained activation of the transcription factor nuclear factor-kappaB, Diabetes 50 (12) (2001) 2792–2808.
[49] C.C. Lin, et al., Methylglyoxal activates NF-kappaB nuclear translocation and induces COX-2 expression via a p38-dependent pathway in synovial cells, Life Sci. 149 (2016) 25–33.
[50] J. Masania, et al., Dicarbonyl stress in clinical obesity, Glycoconj. J. 33 (4) (2016) 581–589.
[51] D.E. Maessen, et al., Delayed intervention with pyridoxamine improves metabolic function and prevents adipose tissue inflammation and insulin resistance in high-fat diet-induced obese mice, Diabetes 65 (4) (2016) 956–966.
[52] S.Y. Li, et al., High-fat diet enhances visceral advanced glycation end products, nuclear O-Glc-Nac modification, p38 mitogen-activated protein kinase activation and apoptosis, Diabetes Obes. Metab. 7 (4) (2005) 448–454.
[53] S.L. Elshaer, et al., Deletion of TXNIP mitigates high-fat diet-impaired angiogenesis and prevents inflammation in a mouse model of critical limb ischemia, Antioxidants (Basel) 6 (3) (2017).
[54] Y.J. Li, et al., Impaired angiogenesis following hind-limb ischemia in diabetes mellitus mice, Chin. Med. Sci. J. 22 (4) (2007) 232–237.
[55] O. Seitz, et al., Wound healing in mice with high-fat diet- or ob gene-induced diabetes-obesity syndromes: a comparative study, Exp. Diabetes Res. 2010 (2010) 476969.
[56] S.P. Tabruyn, A.W. Griffioen, NF-kappa B: a new player in angiostatic therapy, Angiogenesis 11 (1) (2008) 101–106.
[57] M. Swiatkowska, J. Szemraj, C.S. Cierniewski, Induction of PAI-1 expression by tumor necrosis factor alpha in endothelial cells is mediated by its responsive element located in the 4G/5G site, FEBS J. 272 (22) (2005) 5821–5831.
[58] H.W. Chng, et al., A new role for the anti-apoptotic gene A20 in angiogenesis, Exp. Cell Res. 312 (15) (2006) 2897–2907.
[59] P. Chu, et al., Phosphocreatine protects endothelial cells from methylglyoxal induced oxidative stress and apoptosis via the regulation of PI3K/Akt/eNOS and NF-kappaB pathway, Vasc. Pharmacol. 91 (2017) 26–35.